

Opportunities to constrain astrophysical reaction rates for the *s* process through determination of the ground state cross sections

T. Rauscher

Department of Physics, University of Basel, CH-4056 Basel, Switzerland

Thomas.Rauscher@unibas.ch

P. Mohr¹

Diakonie-Klinikum, D-74523 Schwäbisch Hall, Germany

I. Dillmann² and R. Plag³

GSI Helmholtzzentrum für Schwerionenforschung GmbH, D-64291 Darmstadt, Germany

ABSTRACT

Modern models of *s*-process nucleosynthesis in stars require stellar reaction rates with high precision. Most of the neutron capture cross sections in the *s* process have been measured and for an increasing number of reactions the required precision is achieved. This does not necessarily mean, however, that the stellar rates are constrained equally well because only capture on the ground state of a target is measured in the laboratory. Captures on excited states can considerably contribute to stellar rates already at typical *s*-process temperatures. We show that the ground state contribution X to a stellar rate is the relevant measure to identify reactions which are or could be well constrained by experiments and apply it to (n,γ) reactions in the *s* process. It is further shown that the maximally possible reduction in uncertainty of a rate through determination of the g.s. cross section is directly given by X . An error analysis of X is presented and it is found that X is a robust measure with overall small uncertainties. Several specific examples (neutron capture on ^{79}Se , ^{95}Zr , ^{121}Sn , ^{187}Os , and ^{193}Pt) are discussed in detail. The results for a full set of 411 reactions in the *s*-process path are presented in a table to identify reactions to be better constrained by experiments and such which cannot be improved by only measuring ground state cross sections (and thus require supplementary studies). General trends and implications are discussed.

Subject headings: nuclear reactions, nucleosynthesis, abundances

1. Introduction

The astrophysical *s* process is the probably best understood nucleosynthesis process, contributing about half of the natural nuclides beyond Fe

(Käppeler & Mengoni 2006; Straniero, Gallino, & Cristallo 2006; Käppeler et al. 2011). The main component of the *s* process is produced in He-shell flashes of Asymptotic Giant Branch (AGB) stars. A second, weak component is from massive stars, additionally contributing to the nuclei in the mass range $A \lesssim 90$. The *s* process proceeds by sequences of neutron capture reactions to build neutron-richer isotopes within an isotopic chain. As soon as an unstable isotope is reached, β^- -decay moves the

¹Institute of Nuclear Research (ATOMKI), H-4001 Debrecen, Hungary

²II. Physikalisches Institut, Justus-Liebig-Universität, D-35392 Giessen, Germany

³Institut für Angewandte Physik, Goethe-Universität, D-60438 Frankfurt am Main, Germany

synthesis path to the next element with $Z + 1$. In some cases neutron capture and β^- -decay compete because of comparable reaction rates. This establishes branching points in the s -process path. The resulting abundances depend sensitively on the nuclear properties of these branching points. This fact may be used either to derive astrophysical parameters, such as temperature and neutron density during the s process, or to test stellar s -process models which provide these parameters. Furthermore, along isotopic chains in the s -process path it is found that the abundances are inversely proportional to the neutron capture rates.

One prerequisite for the success of nucleosynthesis calculations for the s process is the availability of excellent experimental neutron capture data (see compilations in Bao et al. 2000; Dillmann et al. 2006, 2009). As the s -process path proceeds along the valley of stability, most of the nuclei (except the unstable branching nuclei) can be used as stable targets. Typical s -process temperatures are of the order of $kT \approx 5 - 30$ keV for the main component in the He-shell flashes of AGB stars, where the main neutron source $^{13}\text{C}(\alpha, n)^{16}\text{O}$ operates at the lower end of the temperature range and the second neutron producing reaction $^{22}\text{Ne}(\alpha, n)^{25}\text{Mg}$ at the upper end (Käppeler & Mengoni 2006). The latter reaction at slightly higher temperatures of up to about 80 keV also provides the neutrons for the weak s process component in massive stars (Rauscher et al. 2002). Experiments on stable targets are feasible at these energies, with typical cross sections ranging from milli-barns up to a few barns. However, many reactions on stable targets are still not measured in the full energy range important in the s process. In the near future, also cross section measurements on unstable nuclei in the branchings will become possible.

The central quantities in all s -process calculations are the astrophysical reaction rates. These have to be determined by theoretical predictions in the absence of experimental data in the relevant energy range. Due to the impact of thermal excitation of nuclear states above the ground state in the stellar plasma, however, a theoretical contribution may remain even when the ground state cross sections are measured. Although the s process involves comparatively low plasma temperatures, transitions from low-lying excited states

may contribute considerably to the stellar rate.

We studied the contribution of ground state transitions to stellar neutron capture rates for the s process with the aim to identify cases for which the astrophysical reaction rate is mainly given by the ground state rate and thus can be well constrained by the measurement of ground state cross sections. At the same time this allows to pinpoint reactions for which the uncertainty in the astrophysical reaction rate will not be removed by the determination of ground state cross sections. This is also interesting to s -process modelers who want to estimate the uncertainties in the rates they are using. We also show a general method to determine how the uncertainties in the stellar rates are modified when better constraining one or more transitions from a ground or excited state.

2. Stellar rates

2.1. Definition

Nuclear reactions occurring in an astrophysical plasma are described by astrophysical reaction rates; e.g., for neutron capture the rate is defined by (Fowler 1974; Rauscher 2011)

$$r^* = n_{\text{n}} n_{\text{target}} \langle \sigma v \rangle^* = n_{\text{n}} n_{\text{target}} R^* , \quad (1)$$

with n_{n} , n_{target} being number densities of the neutrons and a species of target nuclei, and the stellar rate factor (also called reactivity) $R^* = \langle \sigma v \rangle^*$. The relative velocities v between the neutrons and the target nuclei are given by the Maxwell-Boltzmann (MB) distribution $\Phi_{\text{MB}}(v, T)$ at temperature T . It can also be expressed as function of relative interaction energy $\Phi(E, T)$.

In a stellar plasma, nuclei are in thermal equilibrium with the plasma. This also implies that internal states can be excited and the nuclei do not have to be in the ground state (g.s.) necessarily, depending on the temperature. In most cases, the excited states within a nucleus are also in thermal equilibrium because the equilibration timescale is short (Gintautas et al. 2009). There are few cases with isomeric or long-lived states that may not be thermalized at s -process temperatures, such as ^{176}Lu (Heil et al. 2008; Mohr et al. 2009; Gintautas et al. 2009) or ^{180}Ta (Belic et al. 1999; Mohr, Käppeler, & Gallino 2007). Assuming thermal equilibrium, the total stellar reactivity

R^* is

$$R^*(T) = w_0 R_0 + w_1 R_1 + w_2 R_2 + \dots \quad (2)$$

with the reactivities of the i -th state in the target

$$R_i(T) = \int_0^\infty \sigma_i(E_i) \Phi(E_i, T) dE_i \quad . \quad (3)$$

The cross section σ_i is the total neutron capture cross section of the i -th state, i.e. summed over all final states j in the residual ($A+1$) nucleus: $\sigma_i = \sum_j \sigma^{i \rightarrow j}$. The relative energy E_i between projectile and target is always measured in the system of the respective target state (i.e., g.s. or excited state) and therefore the integration always starts at zero (Fowler 1974; Rauscher 2011). Thus, the full MB energy distributed neutrons are also acting on nuclei which are in excited states, not only on nuclei in the g.s., and the reaction rate in Eq. (1) has to be defined appropriately by the sum in Eq. (3).

The normalized weights w_i in Eq. (2) of the excited state contributions are given by

$$w_i = \frac{P_i}{\sum_i P_i} = \frac{P_i}{G} \quad , \quad (4)$$

with the partition function $G = \sum_i P_i$ or, normalized to the g.s., $G_0 = G/(2J_0 + 1)$. The population factor P_i of the excited state i with excitation energy E_i and spin J_i is given by the usual Boltzmann factor

$$P_i = (2J_i + 1) \exp\left(-\frac{E_i}{kT}\right) \quad . \quad (5)$$

Normalized partition functions $G_0(T)$ are usually given along with reaction rate predictions and can be found, e.g., in Holmes et al. (1976); Woosley et al. (1976); Rauscher & Thielemann (2000).

Often, the integral in Eq. (3) is divided by the mean thermal velocity $v_{i,T}$, leading to the so-called Maxwellian averaged cross section (MACS). The MACS for the g.s. ($i = 0$) can be derived from a measurement of the neutron capture cross sections over a properly chosen energy interval. This MACS for the g.s. and its uncertainty is provided in the compilations Bao et al. (2000); Dillmann et al. (2006, 2009).

Laboratory experiments are performed on nuclei in the g.s. (with the exception of ^{180}Ta which

is the only naturally occurring isomer and has a short-lived ground state). Thus, experiments only determine the neutron capture cross section of the g.s., i.e., σ_0 . Therefore, only the g.s. reactivity R_0 (or g.s. MACS) can be derived instead of the desired astrophysical reactivity R^* . To assess by how much the g.s. rate differs from the astrophysical rate, usually the so-called “stellar enhancement factor” (SEF)

$$f_{\text{SEF}} = \frac{R^*(T)}{R_0} \quad (6)$$

is used. It is found that the SEF remains relatively close to unity within about 20 – 30 % for most nuclei in the *s*-process path up to temperatures of $kT \approx 100 \text{ keV}$ (Bao et al. 2000; Dillmann et al. 2006, 2009). As shown below, however, this does not necessarily imply a small contribution of transitions from excited states or small remaining uncertainty once R_0 has been well determined.

2.2. Excited state contributions

It can be shown that the weighted sum of integrals in Eq. (2) can be transformed to an integral over a *single* MB distribution (Fowler 1974; Holmes et al. 1976; Rauscher 2011)

$$R^* = \frac{1}{G_0(T)} \int_0^\infty \sigma^{\text{eff}}(E_0) \Phi(E_0, T) dE_0 \quad , \quad (7)$$

thereby avoiding the different energy scales found in Eq. (2). Following Fowler (1974); Holmes et al. (1976), σ^{eff} is the so-called effective cross section, summing over all final states *and* initial excited states up to the interaction energy E

$$\sigma^{\text{eff}}(E) = \sum_i \sum_j \frac{2J_i + 1}{2J_0 + 1} \frac{E - E_i}{E} \sigma^{i \rightarrow j}(E - E_i) \quad . \quad (8)$$

This transformation proves convenient in determining the actual weights with which transitions from excited states i are contributing to the stellar rate. These are not the P_i as defined in Eq. (5) because of the different MB distributions appearing in Eq. (2). They rather are (Rauscher 2011)

$$\mathcal{W}_i = (2J_i + 1) \frac{E - E_i}{E} = (2J_i + 1) \left(1 - \frac{E_i}{E}\right) \quad (9)$$

and therefore *linearly* declining with increasing excitation energy E_i . The energies E appearing in

Eq. (9) are given by the range of energies significantly contributing to the integral in Eq. (7). Therefore the maximum reference energy E appearing is the upper end of the relevant energy window (Gamow window). The relevant energy window for neutron captures is located close to the peak of the MB distribution and its width is comparable to the width of the MB distribution (Iliadis 2007; Rauscher 2010). As can be seen in Iliadis (2007); Rauscher (2010), the upper edge of the effective energy window for neutrons is located not far above the energy $E = kT$, leading to $\mathcal{W}_i \approx (2J_i + 1)(1 - E_i/(kT))$.

The above shows that for the s -process temperature of $kT = 30$ keV, excited states up to $\approx 30 - 40$ keV excitation energy can be important in the target nucleus due to the linearly decreasing weight, for a temperature of $kT = 80$ keV excited states even up to $\approx 80 - 100$ keV have to be considered. Obviously, $\sigma^{i \rightarrow j}$ contains the information on how strong the contribution from the excited state is. But \mathcal{W} allows us to estimate whether we have to bother with calculating $\sigma^{i \rightarrow j}$ at all.

Despite the fact that many nuclei in the s -process path show excited states below 100 keV, especially the heavier nuclides, the SEFs nevertheless remain close to unity for most cases. Clearly, this implies that the (predicted) stellar reactivity is close to the one for the g.s. because either the w_i (\mathcal{W}_i) or the $\sigma^{i \rightarrow j}$ are negligible for $i > 0$, or they conspire to yield a value close to the one obtained for the g.s. transitions alone. The SEF does not allow to distinguish between those cases. For illustration, we examine a nucleus with only two levels characterized by excitation energies $E_0 = 0$ and E_1 , spins J_0 and J_1 , and thermal occupation weights w_0 and w_1 . Let us consider two different cases in this simple model. For case A we assume that 90% of the target nuclei are in the g.s. ($w_0 = 0.9$) and 10% are in the excited state ($w_1 = 0.1$). Let us further assume that the cross section of the excited state σ_1 is proportional to σ_0 , but larger by a factor of two. This yields

$$f_{\text{SEF}}^{\text{A}} = \frac{0.9R_0 + 0.1R_1}{R_0} = 0.9 + 0.1 \times 2 = 1.1 . \quad (10)$$

For case B we assume that 2/3 of the target nuclei are in the first excited state and only 1/3 remain in the g.s. This can be easily achieved for a small excitation energy $E_1 \ll kT$ and $J_0 \ll J_1$. Further,

we assume that the cross section σ_1 is proportional to σ_0 , but larger by 15 %. This results in

$$f_{\text{SEF}}^{\text{B}} = \frac{R_0/3 + 2R_1/3}{R_0} = 1/3 + 2/3 \times 1.15 = 1.1 . \quad (11)$$

Although the SEFs are identical in both cases and close to unity, the essential difference is in the contribution of the excited state, which is small in case A but dominant in case B.

2.3. Ground state contribution

Instead of using the SEF, the importance of excited states in the stellar rate factor R^* can be better assessed by the g.s. contribution X to R^* which is given by

$$X = \frac{w_0 R_0}{R^*} = \frac{w_0}{f_{\text{SEF}}} \quad (12)$$

for the two simple examples above. The quantity X is positive and assumes its maximal value of unity when only the target g.s. is contributing to R^* . It follows that in case A the g.s. contribution to the stellar rate factor is $X = 0.9/1.1 \approx 0.82$, i.e. the stellar rate factor is essentially defined by the dominating g.s. contribution. On the other hand, in case B we find a g.s. contribution of only $X = (1/3)/1.1 \approx 0.30$, i.e. about 70 % of the stellar rate are made by the excited state. This shows that the excited state contribution may exceed the g.s. contribution significantly, even when $f_{\text{SEF}} \approx 1$.

The above result for the g.s. contribution can easily be generalized for many contributing thermally excited states. Equation 7 clearly shows that f_{SEF} is *not* constantly unity without the contribution of excited state transitions but, rather, $f_{\text{SEF}} = 1/G_0$ in this case (Rauscher 2011). Therefore the g.s. contribution $X \leq 1$ in the general case is given by

$$X(T) = \frac{1}{f_{\text{SEF}}(T) G_0(T)} = \frac{R_0}{R^* G_0} . \quad (13)$$

The quantity X will be included in future versions of the KADoNiS compilation (Dillmann et al. 2009). Even when it is not directly given in a compilation, however, it can be easily computed from G_0 and either f_{SEF} or R_0 , as shown above. The SEF itself still retains some interest in the sense that it specifies whether the stellar rate, although incidentally, is similar to the g.s. rate.

2.4. Uncertainty in X

It has to be kept in mind, however, that X itself is a theoretical quantity (like the SEF). The weighted uncertainties in the rates or cross sections of g.s. and excited states determine the total uncertainty in X and f_{SEF} . Entering this total uncertainty, however, are the uncertainties in the *ratios* of the rates of excited states and g.s. as well as the uncertainty in the ratios of the weights, i.e. of G_0 . This can be easily seen when looking at the reciprocal of X (which must have the same relative uncertainty)

$$\frac{1}{X} = 1 + \frac{w_1 R_1}{w_0 R_0} + \frac{w_2 R_2}{w_0 R_0} + \frac{w_3 R_3}{w_0 R_0} + \dots \quad (14)$$

Similar considerations apply to the SEF. For example, using the simple two-level system from section 2.2, we may assign some uncertainty, say a factor of two, to the term $w_1 R_1 / (w_0 R_0)$. This translates into uncertainties $f_{\text{SEF}}^A = 1.1^{+0.20}_{-0.10}$, $X^A = 0.82^{+0.08}_{-0.13}$, and $f_{\text{SEF}}^B = 1.1^{+0.77}_{-0.38}$, $X^B = 0.30^{+0.16}_{-0.12}$.

In the following we study the influence of an uncertainty factor u in the calculations on the resulting ground state contribution X and its inverse $1/X$. Only nuclei at or close to stability participate in the s process. These nuclides have generally well determined level schemes at low excitation energies and therefore G_0 and the weights w_i are well determined. Thus, the uncertainties in X are limited to the uncertainties u_i arising from the predicted ratios R_i/R_0 ,

$$u_{1/X} = 1 + \frac{w_1}{w_0} u_1 \frac{R_1}{R_0} + \frac{w_2}{w_0} u_2 \frac{R_2}{R_0} + \frac{w_3}{w_0} u_3 \frac{R_3}{R_0} + \dots \quad (15)$$

For the two-level system above we had assumed an uncertainty of a factor of two, i.e. $u_1 = 2$ and $u_1 = 1/2$, to arrive at the given total uncertainty in X .

Another convenient property of X is that its uncertainty scales with X itself. This can be seen when assuming $\bar{u} = u_1 = u_2 = u_3 = \dots$ For realistic cases in the s process this is a good approximation to the actual errors in the ratios because only the first few terms in the sum will contribute to X and the weighted average of the uncertainties \bar{u} will be close to the values of u_1 and/or u_2 . The applicability of the assumption can be checked through the normalized partition function. The

closer G_0 is to unity, the better the above assumption holds.

With the above assumption we obtain

$$\begin{aligned} u_{1/X} &= 1 + \bar{u} \left\{ \frac{w_1 R_1}{w_0 R_0} + \frac{w_2 R_2}{w_0 R_0} + \frac{w_3 R_3}{w_0 R_0} + \dots \right\} \\ &= 1 + \bar{u} \left\{ \frac{1}{X} - 1 \right\} . \end{aligned} \quad (16)$$

Then the factor X'/X by which X changes when assuming an averaged uncertainty factor \bar{u} in the rate ratios is

$$u_X = \frac{X'}{X} = \frac{1}{\bar{u}(1-X) + X} . \quad (17)$$

This is an important result as it shows that the uncertainties will be negligible for $X \approx 1$. Uncertainties will be larger for $X \ll 1$ but will still yield $X \ll 1$ when including them. In other words, large X always remain large and very small X remain small. Therefore X is a robust measure of the g.s. contribution and can be used to determine the direct impact of measurements of g.s. cross sections on the astrophysical reaction rate. This is another advantage of using X instead of the SEF. Figure 1 shows the connection between the uncertainty and X .

The uncertainty factor will reach its maximum value $\max(\bar{u}, 1/\bar{u})$ only for very small values of X . It has to be kept in mind that \bar{u} gives the uncertainty in the *ratio* R_i/R_0 and not in the rates or cross sections. Global reaction rate predictions found averaged deviations from measurements of 30% for (n,γ) MACS at 30 keV, with local deviations of up to factors 2 – 3 (Rauscher, Thielemann, & Kratz 1997; Bao et al. 2000). When using locally adjusted parameters, these uncertainties can be reduced further (at the expense of predictive power for unknown nuclides and their properties). It is commonly assumed, however, that the cross section ratios σ_i/σ_0 and thus the reactivity ratios R_i/R_0 are predicted with much smaller uncertainty. This is especially true for the s process. Unknown spins and parities of low-lying states would give rise to the largest part of the uncertainty in the prediction of σ_i/σ_0 but these are known for nuclei at s process conditions. The remaining uncertainty is dominated by the uncertainty in the energy dependence of the γ widths (Rauscher 2010). However, it has to be re-

alized that neutron captures in the *s* process generally have large reaction Q values and therefore the relative change in energy for the contributing transitions $(E - E_i + Q)/Q$ (Rauscher 2008, 2011) when varying E_i is small. This leads to an uncertainty much smaller than the one in the specific cross sections themselves, probably better than 10%.

For a more conservative estimate, the uncertainties in X in table 1 and figures 2, 3 are given for uncertainty factors $\bar{U} = 1.3$, i.e., 30%.

3. Reduction of model uncertainties in stellar rates

3.1. Maximally possible reduction by determining σ_0

The g.s. contribution X to the stellar rate, as derived in section 2.3, is not just of theoretical interest. It directly gives the maximum reduction in the rate uncertainty which can be possibly achieved by completely determining the g.s. rate factor, e.g., by completely measuring the g.s. cross sections σ_0 within the relevant energy window. Assigning an uncertainty factor \mathcal{U} to the theoretically predicted stellar rate R^* , then the perceptual reduction of \mathcal{U} will be simply $100X$ and the new, reduced uncertainty factor

$$\mathcal{U}' = (1 - X)\mathcal{U} . \quad (18)$$

(This assumes the error on the measured σ_0 to be negligible and the cross sections to be known within the full energy range required to compute the reaction rate integral.)

This maximally possible reduction in rate uncertainty is especially important for the *s* process. Both the astrophysical modeling and the cross section measurements have entered a high-precision era, with σ_0 for many targets determined to a few percent precision and stellar models demanding such small uncertainties in the *stellar* rates for a detailed understanding of the production of *s* nuclei and for constraining the conditions within a star. It is important to realize, however, that the stellar rate is constrained with the experimental uncertainty only when $X = 1$. In the extreme case $X \ll 1$ a measurement of g.s. cross sections or MACS will not be able to constrain the rate in any way, even when performed with the highest preci-

sion. In this case R^* is essentially given by the theoretical prediction of the cross sections of the excited states, and further experiments are required to constrain the theoretical predictions. For example, (n,n') reactions for the population of the excited target states (see, e.g., Mosconi et al. 2010b) or (γ,n) reactions on the residual nucleus (e.g., Sonnabend et al. 2003a) have been suggested to study specific transitions to excited states in the target.

It should be noted that even with $X < 1$ the knowledge of σ_0 can be used to test and improve the model prediction of the reaction cross section, even though the measurement will not directly constrain R^* . In many cases, deficiencies in the description of the cross sections of g.s. and excited states are correlated and the prediction of the stellar rate may be improved also in such instances by a renormalization of the rate. Whether this is possible depends on reaction details and has to be investigated separately for each target nucleus.

For completeness it has to be mentioned here that the uncertainties in the SEFs f_{SEF} and ground state contributions X are not the only nuclear uncertainties playing a role in *s*-process nucleosynthesis calculations. In particular, for the interesting branching nuclei often only theoretical predictions of the capture cross sections are available. The feasibility of a considerable reduction of the theoretical uncertainties by measurements can be checked by inspecting X for such nuclei. Furthermore, the branching may be affected by a temperature-dependent β -decay half-life (Takahashi & Yokoi 1987). Also for decay rates (as for any other type of rate) the g.s. contribution can be determined by applying equation 13. In this work, however, we focus on neutron captures close to stability.

3.2. General results

We have calculated SEFs f_{SEF} and g.s. contributions X for a set of nuclides important for *s*-process studies with the reaction rate code SMARAGD, version 0.8.1s (Rauscher 2011). Nuclides present in KADoNiS v0.3 (Dillmann et al. 2009) were supplemented with several additional nuclei under consideration for inclusion in future KADoNiS versions, yielding a set of 411 nuclei. Table 1 shows the considered nuclei with their values of G_0 , X , and f_{SEF} at $kT = 30$ keV and

$kT = 80$ keV (results for further temperatures will be included in future versions of KADoNiS). Also given is the relative uncertainty factor u_X which defines the lower limit $X_{\text{lower}} = X/u_X$ and upper limit $X_{\text{upper}} = u_X X$ of X as discussed in section 2.4. The last column of table 1 provides information on the current experimental status of the (n,γ) reaction on the given target nucleus and identifies the nuclei marked in figure 4 (marked by an asterisk in the comment column). When a reaction is measured (marked by "e") and X is close to unity, the uncertainty in the stellar rate is directly connected to the experimental uncertainty. If X is small, the model uncertainty has not been reduced even when the rate was measured. For several reactions, only a 30 keV MACS was measured (marked by "30") and the rates at other temperatures are determined from a renormalized model calculation. Also listed are reactions with purely theoretical predictions (marked by "t") and such not appearing in KADoNiS v0.3 (marked by "n").

The table is useful for both astrophysicists and experimentalists and is meant to be interpreted as follows. Looking for reactions to better constrain experimentally, those with X close to unity should be chosen. If they were measured previously, it would be possible to better constrain them by measuring with higher precision across the full relevant energy range (see Rauscher 2010). An unmeasured rate will also only be constrained by measuring σ_0 if $X \approx 1$. On the other extreme, some measured reactions show low values for X (marked by the asterisk). It would be incorrect to assume for these cases that the uncertainty of the stellar rate is similar to the one of the measurement. Thus, this allows to assess which reactions presently are well constrained in s process calculations.

For a number of reactions, only $kT = 30$ keV MACS are directly obtained from experiment and the energy dependence taken from theory. Obviously, this will only constrain the stellar rate at 30 keV when $X \approx 1$. Although it is usually preferable to obtain a rate from a measurement within the full range of contributing energies, one has to realize that X may decrease with higher energy, even when it is close to unity at $kT = 30$ keV. In such a case, additional measurements above 30 keV may only partially reduce the uncertainty in the rates

at higher temperature. In order to see the change in X with energy, also values for $kT = 80$ keV are shown in table 1.

For a better overview, further comparisons of g.s. contributions X to (n,γ) rates at different temperatures are shown in figures 2 and 3. We have chosen the reference temperature $kT = 30$ keV for the s process and a high temperature of $T = 2.5$ GK typical for explosive nucleosynthesis. As can be seen, the values of X are smallest in the region of deformed nuclei where also their deviation from the SEF is the largest. This is explained by the fact that the level density in such nuclei is high, i.e., there are already many excited states at low excitation energy. Already at $kT = 30$ keV we find $X \approx 0.16 - 0.3$ for several nuclei (with the lowest values of $X = 0.04$, $X = 0.16$, and $X = 0.2$ for ^{166}Ho , ^{193}Pt , and ^{142}Pr , respectively) and $X \approx 0.5 - 0.8$ for most nuclei in the mass range $150 \leq A \leq 190$. Although experimental data with small uncertainties exist for most stable nuclei in this mass range (Bao et al. 2000; Dillmann et al. 2006, 2009), the stellar reactivity R^* is at least partially based on the calculated contribution of excited states. Consequently, the uncertainties of the stellar reactivities R^* may be much larger than the uncertainties of the ground state MACS which are provided in the compilations Bao et al. (2000); Dillmann et al. (2006, 2009).

At a glance, figure 4 provides a guide to which targets are well suited for experimentally constraining the model uncertainties and which are not. The filled squares mark nuclei with $X < 0.8$ (using the lower limit of X from the errors discussed in section 2.4). For neutron captures on these targets, even a complete experimental determination of the g.s. rates will not be able to reduce the model error by more than 80% and for even smaller X it will not provide an improved rate. The open squares mark nuclei in our set having $X \geq 0.8$ and therefore show cases for which the rate uncertainty mainly stems from experimental uncertainties. If not measured already, they may provide good opportunities for future experiments.

The cut at 80% error reduction was chosen because a significant reduction in model uncertainty is required in order to achieve the precision desired for s -process nucleosynthesis. For example, assuming a 80% reduction in an uncertainty of 30% in the rate predictions (Rauscher, Thielemann, & Kratz

1997), the remaining error stemming from theory will then be of the order of 6%. Assuming larger factors of 2 – 3 in global reaction rate predictions reduced by 80% would lead to a theory uncertainty in the stellar rate of about 40 – 60% from the excited state contributions. The experimental uncertainty for σ_0 has to be additionally included. This leads to uncertainties in stellar rates which already may be too large for high-precision *s*-process nucleosynthesis models.

Neutron captures and their inverse photodisintegration reactions at higher temperatures are also important in the γ -process production of *p* nuclei (Woosley & Howard 1978; Rauscher 2006). For that reason, they are also included in KADoNiS (Dillmann et al. 2009). It is apparent in figure 3 that X can assume very low values for higher temperature. This indicates that one has to be very careful in extrapolating experimental rates from *s*-process temperatures ($T = 0.384$ GK is $E = 30$ keV), e.g., to a typical γ -process temperature of 2.5 GK. This implies an increasing theory contribution which is only constrained by experiment, as pointed out above, if the predictions of the g.s. and excited state cross sections are correlated. Furthermore, while the partition function G_0 is well determined at *s*-process conditions by experimentally known level schemes, going to higher temperature (and/or unstable nuclei) implies an increasing uncertainty also in G_0 .

3.3. Specific examples

Finally, let us discuss some specific cases in more detail to further illustrate the difference between f_{SEF} and X : neutron capture reactions on ^{79}Se , ^{95}Zr , ^{121}Sn , ^{187}Os , and ^{193}Pt . We focus here on the stellar temperatures $kT = 8$ keV and $kT = 30$ keV. A temperature of $kT = 30$ keV is often taken as the reference temperature of the *s* process (see, e.g., Dillmann et al. 2009). It is close to the typical burning temperature of the $^{22}\text{Ne}(\alpha, \text{n})^{25}\text{Mg}$ reaction which is one of the two neutron sources for the *s* process in thermally pulsing AGB stars. The main neutron source in AGB stars is $^{13}\text{C}(\alpha, \text{n})^{16}\text{O}$ which operates at lower temperatures around $kT = 8$ keV. Already at these relatively low temperatures the g.s. contribution X to the stellar reaction rate factor R^* is far below unity in some cases. The weak *s* process in massive stars operates at higher temperatures, and

thus the ground state contribution X is even further reduced.

The reaction $^{79}\text{Se}(\text{n}, \gamma)^{80}\text{Se}$ is an example of a case where $f_{\text{SEF}} < 1$ due to a weak influence of excited states. The nucleus ^{79}Se has several low-lying levels ($J^\pi = 1/2^-$, 95.8 keV; $(1/2^-)$, 128 keV(?); $9/2^+$, 137.0 keV) above its $7/2^+$ g.s. (Singh 2002; ENSDF 2010). Because of $J_0 = 7/2$ and $J_1 = 1/2$ of the first excited state, its population remains below about 1% up to $kT = 30$ keV, and a similar value is found for the large $J = 9/2$ state at 137.0 keV. This leads to $G_0 = 1.027$, $f_{\text{SEF}} = 0.99$, and $X = 0.98$ at $kT = 30$ keV. Moreover, ^{79}Se is considered as an important branching nucleus with a highly temperature-dependent half-life (Takahashi & Yokoi 1987) in the weak *s* process. For $kT = 100$ keV we find $f_{\text{SEF}} = 0.85$ and $X = 0.78$. This means that not only the excited states are populated more ($G_0 = 1.51$) but also the captures on these states impact the resulting stellar rate. Were this not the case, i.e., were the capture cross sections of ^{79}Se in the excited states negligible, then $X = 1$ and $f_{\text{SEF}} = 1/G_0 = 0.66$.

The reaction $^{95}\text{Zr}(\text{n}, \gamma)^{96}\text{Zr}$ is an example of both $f_{\text{SEF}} = 1$ and $X = 1$ because excited states are not populated. The first excited state of ^{95}Zr is located at $E = 954$ keV with $J^\pi = 1/2^+$. The g.s. has $J^\pi = 5/2^+$ (ENSDF 2010). The SEF and X do not deviate from unity over the whole temperature range of the *s* process because $G_0(T) = 1$. Note that there was an earlier claim for a low-lying first excited state with $J^\pi = (3/2, 5/2)^+$ at 23 keV which has been observed only in one particular experiment (Frota-Pessôa & Joffily 1986). The existence of such a level has been excluded in a later high-resolution experiment (Sonnabend et al. 2003b). There is no evidence for another low-lying state “with quite different angular momentum” as discussed recently in Huther et al. (2010). Consequently, the state at 23 keV has been removed from the adopted levels of ^{95}Zr (Basu, Mukherjee, & Sonzogni 2010; ENSDF 2010). An experimental determination of the $^{95}\text{Zr}(\text{n}, \gamma)^{96}\text{Zr}$ capture cross section would be extremely valuable because the experimental neutron capture data completely define the stellar reaction rate. These data are a prerequisite for the understanding of isotopic patterns of zirconium and molybdenum isotopes in meteorites which may be of *s*-process origin.

The reaction $^{121}\text{Sn}(\text{n},\gamma)^{122}\text{Sn}$ is close to our example B above. The g.s. of ^{121}Sn has a low spin of $J^\pi = 3/2^+$. There is a very low-lying intruder state at $E = 6.3$ keV with $J^\pi = 11/2^-$, and a further low- J state at $E = 60.3$ keV with $J^\pi = 1/2^+$. Then there is a gap in the level scheme up to the next state at $E = 663.6$ keV which is too high to play a significant role for the s process (Ohya 2010; ENSDF 2010). Already at $kT = 8$ keV the population of the first excited state exceeds the g.s., and we find a g.s. contribution to the stellar rate of $X = 0.36$. At the reference temperature of $kT = 30$ keV it is further reduced to $X = 0.27$. The SEFs remain close to unity with $f_{\text{SEF}} = 1.19$ and 1.07 at 8 keV and 30 keV. Because of the dominating contribution from the first excited state, experimental data for the $^{121}\text{Sn}(\text{n},\gamma)^{122}\text{Sn}$ reaction can only determine a minor contribution of one third to the stellar rate.

The reaction $^{187}\text{Os}(\text{n},\gamma)^{188}\text{Os}$ is important for the Re/Os cosmochronometer (Mosconi et al. 2010a,b). The nucleus ^{187}Os exhibits a very low-lying $3/2^-$ state at 9.8 keV above the $1/2^-$ g.s. The next levels appear at 74.4 keV, 75.0 keV, and 100.5 keV ($3/2^-$, $5/2^-$, $7/2^-$). Above a level at 117 keV without spin assignment the next levels are found at 187.4 keV and 190.6 keV, which is too high for the s process (Basunia 2009; ENSDF 2010). At $kT = 8$ keV the SEF is $f_{\text{SEF}} = 1.0$. The first excited state, however, is already populated and we find a g.s. contribution of $X = 0.63$. At higher energies the g.s. contribution reduces further to $X = 0.28$ for $kT = 30$ keV, although $f_{\text{SEF}} = 1.19$ remains close to unity. Because of the relevance of this reaction for the Re/Os cosmochronometer, neutron capture experiments on ^{187}Os have been performed (see, e.g., Mosconi et al. 2010a; Fujii et al. 2010, and references therein). The importance of the low-lying first excited state has been noticed in that work and additional experiments on inelastic neutron scattering of ^{187}Os and photodisintegration of ^{188}Os have been performed (see, e.g., Shizuma et al. 2005; Mosconi et al. 2010b) to study transitions proceeding on this state.

Another example for the importance of including excited state transitions is $^{193}\text{Pt}(\text{n},\gamma)^{194}\text{Pt}$. An extremely low-lying $3/2^-$ state at $E = 1.6$ keV is found above the $1/2^-$ g.s. of ^{193}Pt , and a further low-lying $5/2^-$ state is located at $E = 14.3$

keV. Then there is a small gap in the level scheme up to the next $3/2^-$ state at $E = 114.2$ keV (Achterberg et al. 2006; ENSDF 2010). Already at $kT = 8$ keV the first excited state is dominating the reaction rate factor R^* and the g.s. contribution is only $X = 0.26$. At $kT = 30$ keV the g.s. contribution drops to $X = 0.16$, and the reactivity R^* is essentially determined by comparable contributions of the states at 1.6 keV and 14.3 keV. Again, as in the previous examples, the SEF remains relatively close to unity with $f_{\text{SEF}} = 1.22$ at $kT = 8$ keV and $f_{\text{SEF}} = 1.31$ at $kT = 30$ keV. Thus, an experimental determination of the $^{193}\text{Pt}(\text{n},\gamma)^{194}\text{Pt}$ cross section can only be used to restrict theoretical predictions for the g.s. cross section. Similarly to the above examples ^{121}Sn and ^{187}Os , it is not possible to directly derive the stellar reaction rate from experimental neutron capture data.

4. Summary

In conclusion, SEFs close to unity should not be interpreted as that thermally excited states play only a minor role in the stellar reaction rate. The g.s. contribution X to the stellar reaction rate – given by $X = (f_{\text{SEF}} G_0)^{-1}$ – may be significantly below 0.5 for target nuclei with low-lying excited states also for cases with $f_{\text{SEF}} \approx 1$. Low values of X indicate that it is impossible to determine the stellar reaction rate directly from experimental neutron capture data. This should be taken into account in the planning of future neutron capture experiments, in particular for the extremely difficult experiments on unstable branching nuclei in the s process. Because of the importance of the g.s. contribution X , it will be included in future versions of the KADoNiS database (Dillmann et al. 2006, 2009).

Although X is a theoretical quantity, it was shown that the uncertainties of X remain relatively small for most nuclei on the s -process path because the partition functions can be calculated from the experimentally well-known level scheme for these nuclei.

Obviously, these findings apply not only to neutron capture but to any kind of reaction, also in other nucleosynthesis processes. Especially at the high temperatures of explosive nucleosynthesis, reactions on nuclei in excited states often contribute

significantly to the stellar rate. Only the g.s. contribution X , which can be calculated in the same manner for all types of reactions, allows to judge whether measurements of reactions on nuclei in the g.s. will be able to put direct constraints on the stellar rate.

This work was supported by OTKA (NN83261). I.D. and R.P. are supported by the Helmholtz association in the Young Investigators projects VH-NG-627 and VH-NG-327. T.R. receives support from the THE XO workpackage of the ENSAR project within the European Commission FP7.

REFERENCES

- Achterberg, E., Capurro, O. A., Marti, G. V., Vanin, V. R., & Castro, R. M. 2006, Nucl. Data Sheets, 107, 1
- Bao, Z. Y., Beer, H., Käppeler, F., Voss, F., Wissak, K., & Rauscher, T. 2000, At. Data Nucl. Data Tables, 76, 70
- Basu, S. K., Mukherjee, G., & Sonzogni, A. A. 2010, Nucl. Data Sheets, 111, 2555
- Basunia, M. S. 2009, Nucl. Data Sheets, 110, 999
- Belic, D., et al. 1999, Phys. Rev. Lett., 83, 5242
- Dillmann, I., Heil, M., Käppeler, F., Plag, R., Rauscher, T., & Thielemann, F.-K. 2006, AIP Conf. Proc., 819, 123
- Dillmann, I., Plag, R., Käppeler, F., & Rauscher, T. 2009 Proc. of "EFNUDAT Fast Neutrons - scientific workshop on neutron measurements, theory & applications", April 28-30 2009, Geel, Belgium; available at www.kadonis.org.
- ENSDF 2010, (<http://www.nndc.bnl.gov/ensdf/>) online database; based on Singh (2002) for ^{79}Se , Basu, Mukherjee, & Sonzogni (2010) for ^{95}Zr , Ohya (2010) for ^{121}Sn , Basunia (2009) for ^{187}Os , and Achterberg et al. (2006) for ^{193}Pt .
- Fowler, W. A. 1974, QJRAS, 15, 82
- Frota-Pessôa, E. & Joffily, S. 1986, Nuovo Cimento, 91A, 370
- Fujii, K., et al. 2010, Phys. Rev. C, 82, 015804
- Gintautas, V., Champagne, A. E., Kondev, F. G., & Longland, R. 2009, Phys. Rev. C, 80, 015806
- Heil, M., et al. 2008, ApJ, 673, 434
- Holmes, J. A., Woosley, S. E., Fowler, W. A., & Zimmerman, B. A. 1976, At. Data Nucl. Data Tables, 18, 305
- Huther, L., Loens, H. P., Martínez-Pinedo, G., & Langanke, K. 2010, Europ. Phys. J. A, 47, 10
- Iliadis, C. 2007, Nuclear Physics of Stars (Wiley, Weinheim)
- Käppeler, F., Gallino, R., Bisterzo, S., & Aoki, W. 2011, Rev. Mod. Phys., 83, 157
- Käppeler, F. & Mengoni, A. 2006, Nucl. Phys., A777, 291
- Mohr, P., Bisterzo, S., Gallino, R., Käppeler, F., Kneissl, U., & Winckler, N. 2009 Phys. Rev. C, 79, 045804
- Mohr, P., Käppeler, F., & Gallino, R. 2007, Phys. Rev. C, 75, 012802(R)
- Mosconi, M., et al. 2010a, Phys. Rev. C, 82, 015802
- Mosconi, M., et al. 2010b, Phys. Rev. C, 82, 015803
- Ohya, S. 2010, Nucl. Data Sheets, 111, 1619
- Rauscher, T. 2006, Phys. Rev. C, 73, 015804
- Rauscher, T. 2008, Phys. Rev. C, 78, 032801(R)
- Rauscher, T. 2010, Phys. Rev. C, 81, 045807
- Rauscher, T. 2011, Int. J. Mod. Phys. E, 20, in press; arXiv:1010.4283.
- Rauscher, T., Heger, A., Hoffman, R. D. & Woosley, S. E. 2002, ApJ, 576, 323
- Rauscher, T. & Thielemann, F.-K. 2000, At. Data Nucl. Data Tables, 75, 1
- Rauscher, T., Thielemann, F.-K., & Kratz, K.-L. 1997, Phys. Rev. C, 56, 1613
- Shizuma, T., et al. 2005, Phys. Rev. C, 72, 025808
- Singh, B. 2002, Nucl. Data Sheets, 96, 1

- Sonnabend, K., et al. 2003a, ApJ, 583, 506
- Sonnabend, K., Mohr, P., Zilges, A., Hertenberger, R., Wirth, H.-F., Graw, G., & Faester-mann, T. 2003b, Phys. Rev. C, 68, 048802
- Straniero, O., Gallino, R., & Cristallo, S. 2006, Nucl. Phys., A777, 311
- Takahashi, K. & Yokoi, K. 1987, At. Data Nucl. Data Tables, 36, 375
- Woosley, S. E., Fowler, W. A., Holmes, J. A., & Zimmerman, B. A. 1976, At. Data Nucl. Data Tables, 22, 371
- Woosley, S. E. & Howard, W. M. 1978, ApJS, 36, 285

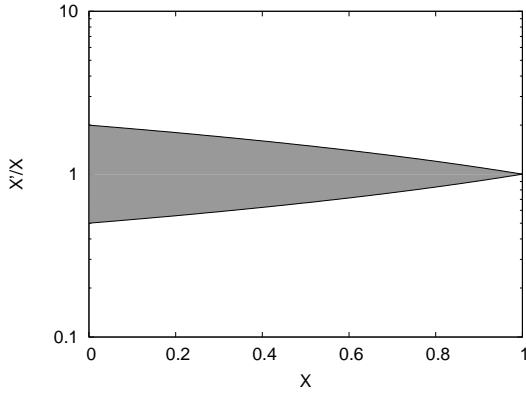


Fig. 1.— Scaling of the uncertainty in X with X . Shown is the ratio X'/X when assuming an averaged uncertainty factor \bar{u} of two. See text for a discussion.

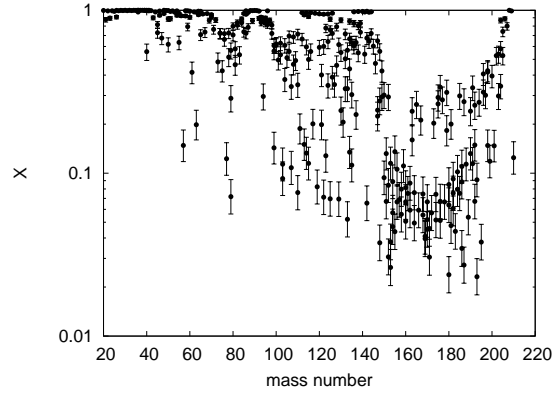


Fig. 3.— Same as figure 2 but for $T = 2.5$ GK. Note the logarithmic scale.

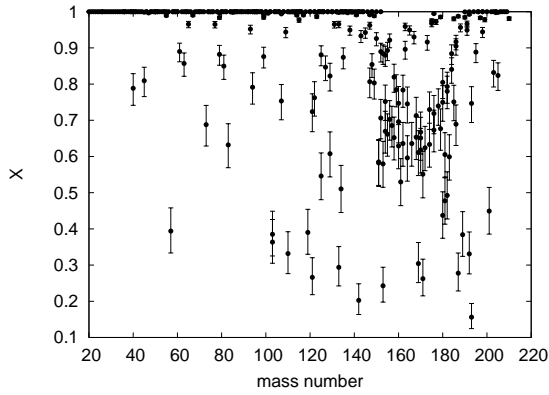


Fig. 2.— Ground state contributions X to the stellar (n,γ) rate at $kT = 30$ keV or $T = 0.384$ GK for our set of nuclides for s process calculations (see text).

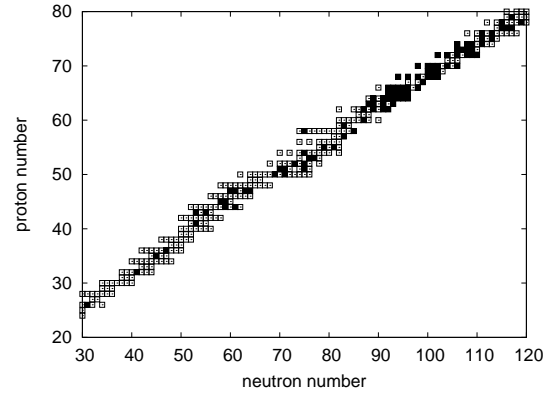


Fig. 4.— The open squares are all nuclides contained in our set for the s process (see text). The black squares mark nuclei for which $X_{\text{lower}} < 0.8$ and therefore an experimental measurement of g.s. cross sections cannot reduce the theoretical uncertainty by more than 80%.

TABLE 1

NORMALIZED PARTITION FUNCTIONS G_0 , GROUND STATE CONTRIBUTIONS X , THEIR UNCERTAINTY FACTORS u_X , AND STELLAR ENHANCEMENT FACTORS f_{SEF} AT $kT = 30$ KEV AND $kT = 80$ KEV FOR NUCLIDES IDENTIFIED BY THEIR CHARGE NUMBER Z AND MASS NUMBER A .

Z	A	Nucl.	G_0^{30}	X^{30}	u_X^{30}	f_{SEF}^{30}	G_0^{80}	X^{80}	u_X^{80}	f_{SEF}^{80}	Comment ^a
10	20	^{20}Ne	1.000	1.000	1.000	1.000	1.000	1.000	1.000	1.000	e
10	21	^{21}Ne	1.000	1.000	1.000	1.000	1.019	0.993	1.002	0.988	e
10	22	^{22}Ne	1.000	1.000	1.000	1.000	1.000	1.000	1.000	1.000	30
11	23	^{23}Na	1.000	1.000	1.000	1.000	1.006	0.997	1.001	0.997	e
12	24	^{24}Mg	1.000	1.000	1.000	1.000	1.000	1.000	1.000	1.000	e
12	25	^{25}Mg	1.000	1.000	1.000	1.000	1.000	1.000	1.000	1.000	e
12	26	^{26}Mg	1.000	1.000	1.000	1.000	1.000	1.000	1.000	1.000	e
13	26	^{26}Al	1.000	1.000	1.000	1.000	1.009	0.995	1.001	0.996	t
13	27	^{27}Al	1.000	1.000	1.000	1.000	1.000	1.000	1.000	1.000	e
14	28	^{28}Si	1.000	1.000	1.000	1.000	1.000	1.000	1.000	1.000	e
14	29	^{29}Si	1.000	1.000	1.000	1.000	1.000	1.000	1.000	1.000	e
14	30	^{30}Si	1.000	1.000	1.000	1.000	1.000	1.000	1.000	1.000	e
15	31	^{31}P	1.000	1.000	1.000	1.000	1.000	1.000	1.000	1.000	e
15	32	^{32}P	1.123	0.945	1.013	0.943	1.628	0.719	1.069	0.855	n
15	33	^{33}P	1.000	1.000	1.000	1.000	1.000	1.000	1.000	1.000	n
16	32	^{32}S	1.000	1.000	1.000	1.000	1.000	1.000	1.000	1.000	e
16	33	^{33}S	1.000	1.000	1.000	1.000	1.000	1.000	1.000	1.000	e
16	34	^{34}S	1.000	1.000	1.000	1.000	1.000	1.000	1.000	1.000	e
16	35	^{35}S	1.000	1.000	1.000	1.000	1.000	1.000	1.000	1.000	n
16	36	^{36}S	1.000	1.000	1.000	1.000	1.000	1.000	1.000	1.000	e
17	35	^{35}Cl	1.000	1.000	1.000	1.000	1.000	1.000	1.000	1.000	e
17	36	^{36}Cl	1.000	1.000	1.000	1.000	1.000	1.000	1.000	1.000	t
17	37	^{37}Cl	1.000	1.000	1.000	1.000	1.000	1.000	1.000	1.000	e
18	36	^{36}Ar	1.000	1.000	1.000	1.000	1.000	1.000	1.000	1.000	t
18	37	^{37}Ar	1.000	1.000	1.000	1.000	1.000	1.000	1.000	1.000	n
18	38	^{38}Ar	1.000	1.000	1.000	1.000	1.000	1.000	1.000	1.000	t
18	39	^{39}Ar	1.000	1.000	1.000	1.000	1.000	1.000	1.000	1.000	t
18	40	^{40}Ar	1.000	1.000	1.000	1.000	1.000	1.000	1.000	1.000	30
19	39	^{39}K	1.000	1.000	1.000	1.000	1.000	1.000	1.000	1.000	e
19	40	^{40}K	1.288	0.788	1.051	0.985	1.536	0.636	1.092	1.024	t,*
19	41	^{41}K	1.000	1.000	1.000	1.000	1.000	1.000	1.000	1.000	e
20	40	^{40}Ca	1.000	1.000	1.000	1.000	1.000	1.000	1.000	1.000	30
20	41	^{41}Ca	1.000	1.000	1.000	1.000	1.000	1.000	1.000	1.000	t
20	42	^{42}Ca	1.000	1.000	1.000	1.000	1.000	1.000	1.000	1.000	e
20	43	^{43}Ca	1.000	1.000	1.000	1.000	1.007	0.995	1.001	0.998	e
20	44	^{44}Ca	1.000	1.000	1.000	1.000	1.000	1.000	1.000	1.000	e
20	45	^{45}Ca	1.002	0.999	1.000	0.999	1.085	0.954	1.011	0.966	t
20	46	^{46}Ca	1.000	1.000	1.000	1.000	1.000	1.000	1.000	1.000	e
20	47	^{47}Ca	1.000	1.000	1.000	1.000	1.000	1.000	1.000	1.000	n
20	48	^{48}Ca	1.000	1.000	1.000	1.000	1.000	1.000	1.000	1.000	e
21	45	^{45}Sc	1.331	0.809	1.046	0.929	1.434	0.765	1.057	0.912	e,*

TABLE 1—Continued

Z	A	Nucl.	G_0^{30}	X^{30}	u_X^{30}	f_{SEF}^{30}	G_0^{80}	X^{80}	u_X^{80}	f_{SEF}^{80}	Comment ^a
21	46	^{46}Sc	1.259	0.917	1.019	0.866	1.910	0.737	1.065	0.711	n
21	47	^{47}Sc	1.000	1.000	1.000	1.000	1.000	1.000	1.000	1.000	n
21	48	^{48}Sc	1.011	0.988	1.003	1.001	1.199	0.798	1.049	1.045	n
22	46	^{46}Ti	1.000	1.000	1.000	1.000	1.000	1.000	1.000	1.000	e
22	47	^{47}Ti	1.007	0.997	1.001	0.997	1.187	0.906	1.022	0.930	e
22	48	^{48}Ti	1.000	1.000	1.000	1.000	1.000	1.000	1.000	1.000	e
22	49	^{49}Ti	1.000	1.000	1.000	1.000	1.000	1.000	1.000	1.000	e
22	50	^{50}Ti	1.000	1.000	1.000	1.000	1.000	1.000	1.000	1.000	e
23	50	^{50}V	1.000	1.000	1.000	1.000	1.072	0.939	1.014	0.994	t
23	51	^{51}V	1.000	1.000	1.000	1.000	1.015	0.992	1.002	0.993	e
24	50	^{50}Cr	1.000	1.000	1.000	1.000	1.000	1.000	1.000	1.000	e
24	51	^{51}Cr	1.000	1.000	1.000	1.000	1.000	1.000	1.000	1.000	t
24	52	^{52}Cr	1.000	1.000	1.000	1.000	1.000	1.000	1.000	1.000	e
24	53	^{53}Cr	1.000	1.000	1.000	1.000	1.000	1.000	1.000	1.000	e
24	54	^{54}Cr	1.000	1.000	1.000	1.000	1.000	1.000	1.000	1.000	e
25	55	^{55}Mn	1.020	0.989	1.002	0.991	1.276	0.859	1.034	0.912	e
26	54	^{54}Fe	1.000	1.000	1.000	1.000	1.000	1.000	1.000	1.000	e
26	55	^{55}Fe	1.000	1.000	1.000	1.000	1.003	0.999	1.000	0.998	t
26	56	^{56}Fe	1.000	1.000	1.000	1.000	1.000	1.000	1.000	1.000	e
26	57	^{57}Fe	2.269	0.394	1.163	1.118	3.236	0.248	1.210	1.246	e,*
26	58	^{58}Fe	1.000	1.000	1.000	1.000	1.000	1.000	1.000	1.000	e
26	60	^{60}Fe	1.000	1.000	1.000	1.000	1.000	1.000	1.000	1.000	30
27	59	^{59}Co	1.000	1.000	1.000	1.000	1.000	1.000	1.000	1.000	e
27	60	^{60}Co	1.065	0.909	1.022	1.034	1.268	0.746	1.062	1.058	n
28	58	^{58}Ni	1.000	1.000	1.000	1.000	1.000	1.000	1.000	1.000	e
28	59	^{59}Ni	1.000	1.000	1.000	1.000	1.023	0.986	1.003	0.991	t
28	60	^{60}Ni	1.000	1.000	1.000	1.000	1.000	1.000	1.000	1.000	e
28	61	^{61}Ni	1.159	0.890	1.026	0.970	1.661	0.624	1.095	0.966	e
28	62	^{62}Ni	1.000	1.000	1.000	1.000	1.000	1.000	1.000	1.000	30
28	63	^{63}Ni	1.175	0.857	1.034	0.993	2.298	0.437	1.149	0.996	t
28	64	^{64}Ni	1.000	1.000	1.000	1.000	1.000	1.000	1.000	1.000	e
29	63	^{63}Cu	1.000	1.000	1.000	1.000	1.000	1.000	1.000	1.000	e
29	64	^{64}Cu	1.008	0.992	1.002	0.999	1.321	0.790	1.051	0.958	n
29	65	^{65}Cu	1.000	1.000	1.000	1.000	1.000	1.000	1.000	1.000	e
30	64	^{64}Zn	1.000	1.000	1.000	1.000	1.000	1.000	1.000	1.000	e
30	65	^{65}Zn	1.070	0.966	1.008	0.968	1.378	0.863	1.033	0.840	t
30	66	^{66}Zn	1.000	1.000	1.000	1.000	1.000	1.000	1.000	1.000	e
30	67	^{67}Zn	1.016	0.990	1.002	0.994	1.176	0.924	1.018	0.920	e
30	68	^{68}Zn	1.000	1.000	1.000	1.000	1.000	1.000	1.000	1.000	e
30	69	^{69}Zn	1.000	1.000	1.000	1.000	1.025	0.975	1.006	1.000	n
30	70	^{70}Zn	1.000	1.000	1.000	1.000	1.000	1.000	1.000	1.000	t

TABLE 1—Continued

<i>Z</i>	<i>A</i>	Nucl.	G_0^{30}	X^{30}	u_X^{30}	f_{SEF}^{30}	G_0^{80}	X^{80}	u_X^{80}	f_{SEF}^{80}	Comment ^a
31	69	^{69}Ga	1.000	1.000	1.000	1.000	1.010	0.996	1.001	0.994	e
31	70	^{70}Ga	1.000	1.000	1.000	1.000	1.004	0.997	1.001	0.999	n
31	71	^{71}Ga	1.000	1.000	1.000	1.000	1.010	0.996	1.001	0.995	30
32	70	^{70}Ge	1.000	1.000	1.000	1.000	1.000	1.000	1.000	1.000	e
32	71	^{71}Ge	1.016	0.982	1.004	1.002	1.767	0.530	1.122	1.067	n
32	72	^{72}Ge	1.000	1.000	1.000	1.000	1.000	1.000	1.000	1.000	t
32	73	^{73}Ge	1.488	0.688	1.078	0.977	1.952	0.575	1.109	0.891	t,*
32	74	^{74}Ge	1.000	1.000	1.000	1.000	1.003	0.996	1.001	1.001	30
32	75	^{75}Ge	1.050	0.956	1.010	0.996	2.536	0.463	1.141	0.851	n
32	76	^{76}Ge	1.000	1.000	1.000	1.000	1.004	0.996	1.001	1.000	30
33	75	^{75}As	1.001	1.000	1.000	0.999	1.193	0.900	1.024	0.931	e
33	76	^{76}As	1.198	0.910	1.021	0.917	2.168	0.640	1.091	0.721	n
33	77	^{77}As	1.002	0.999	1.000	0.998	1.219	0.920	1.019	0.891	n
34	74	^{74}Se	1.000	1.000	1.000	1.000	1.002	0.997	1.001	1.001	30
34	75	^{75}Se	1.051	0.968	1.007	0.983	1.677	0.696	1.076	0.858	n
34	76	^{76}Se	1.000	1.000	1.000	1.000	1.005	0.994	1.001	1.001	e
34	77	^{77}Se	1.034	0.965	1.008	1.002	2.409	0.430	1.151	0.965	t
34	78	^{78}Se	1.000	1.000	1.000	1.000	1.002	0.997	1.001	1.001	30
34	79	^{79}Se	1.027	0.984	1.004	0.990	1.361	0.836	1.039	0.879	t
34	80	^{80}Se	1.000	1.000	1.000	1.000	1.001	0.999	1.000	1.000	e
34	81	^{81}Se	1.129	0.848	1.036	1.044	2.244	0.356	1.175	1.253	n
34	82	^{82}Se	1.000	1.000	1.000	1.000	1.001	0.999	1.000	1.000	t
35	79	^{79}Br	1.004	0.997	1.001	1.000	1.354	0.763	1.058	0.968	e
35	80	^{80}Br	1.696	0.582	1.107	1.012	3.893	0.226	1.217	1.136	n,*
35	81	^{81}Br	1.000	1.000	1.000	1.000	1.053	0.961	1.009	0.989	e
35	82	^{82}Br	1.121	0.904	1.023	0.987	1.397	0.777	1.054	0.921	n
36	78	^{78}Kr	1.000	1.000	1.000	1.000	1.017	0.978	1.005	1.006	e
36	79	^{79}Kr	1.115	0.882	1.028	1.017	3.383	0.265	1.204	1.115	t
36	80	^{80}Kr	1.000	1.000	1.000	1.000	1.002	0.997	1.001	1.001	e
36	81	^{81}Kr	1.240	0.850	1.036	0.949	1.700	0.637	1.092	0.924	t
36	82	^{82}Kr	1.000	1.000	1.000	1.000	1.000	1.000	1.000	1.000	e
36	83	^{83}Kr	1.635	0.632	1.093	0.968	1.831	0.564	1.112	0.968	e,*
36	84	^{84}Kr	1.000	1.000	1.000	1.000	1.000	1.000	1.000	1.000	e
36	85	^{85}Kr	1.000	1.000	1.000	1.000	1.004	0.996	1.001	1.000	t
36	86	^{86}Kr	1.000	1.000	1.000	1.000	1.000	1.000	1.000	1.000	e
37	85	^{85}Rb	1.004	0.998	1.000	0.997	1.113	0.956	1.010	0.939	e
37	86	^{86}Rb	1.000	1.000	1.000	1.000	1.005	0.996	1.001	0.999	t
37	87	^{87}Rb	1.000	1.000	1.000	1.000	1.010	0.993	1.002	0.997	e
38	84	^{84}Sr	1.000	1.000	1.000	1.000	1.000	1.000	1.000	1.000	30
38	85	^{85}Sr	1.000	1.000	1.000	1.000	1.054	0.966	1.008	0.981	n
38	86	^{86}Sr	1.000	1.000	1.000	1.000	1.000	1.000	1.000	1.000	e

TABLE 1—Continued

Z	A	Nucl.	G_0^{30}	X^{30}	u_X^{30}	f_{SEF}^{30}	G_0^{80}	X^{80}	u_X^{80}	f_{SEF}^{80}	Comment ^a
38	87	^{87}Sr	1.000	1.000	1.000	1.000	1.002	0.999	1.000	1.000	e
38	88	^{88}Sr	1.000	1.000	1.000	1.000	1.000	1.000	1.000	1.000	e
38	89	^{89}Sr	1.000	1.000	1.000	1.000	1.000	1.000	1.000	1.000	t
38	90	^{90}Sr	1.000	1.000	1.000	1.000	1.000	1.000	1.000	1.000	n
39	89	^{89}Y	1.000	1.000	1.000	1.000	1.000	1.000	1.000	1.000	e
39	90	^{90}Y	1.002	0.999	1.000	1.000	1.112	0.918	1.019	0.980	n
39	91	^{91}Y	1.000	1.000	1.000	1.000	1.005	0.992	1.002	1.003	n
40	90	^{90}Zr	1.000	1.000	1.000	1.000	1.000	1.000	1.000	1.000	e
40	91	^{91}Zr	1.000	1.000	1.000	1.000	1.000	1.000	1.000	1.000	30
40	92	^{92}Zr	1.000	1.000	1.000	1.000	1.000	1.000	1.000	1.000	e
40	93	^{93}Zr	1.000	1.000	1.000	1.000	1.024	0.992	1.002	0.985	e
40	94	^{94}Zr	1.000	1.000	1.000	1.000	1.000	1.000	1.000	1.000	e
40	95	^{95}Zr	1.000	1.000	1.000	1.000	1.001	0.999	1.000	1.000	t
40	96	^{96}Zr	1.000	1.000	1.000	1.000	1.000	1.000	1.000	1.000	e
41	93	^{93}Nb	1.072	0.952	1.011	0.980	1.136	0.915	1.020	0.962	e
41	94	^{94}Nb	1.342	0.791	1.051	0.942	2.382	0.493	1.132	0.851	t,*
41	95	^{95}Nb	1.000	1.000	1.000	1.000	1.011	0.990	1.002	0.999	t
41	96	^{96}Nb	1.201	0.862	1.033	0.966	1.716	0.625	1.095	0.933	n
42	92	^{92}Mo	1.000	1.000	1.000	1.000	1.000	1.000	1.000	1.000	e
42	93	^{93}Mo	1.000	1.000	1.000	1.000	1.000	1.000	1.000	1.000	n
42	94	^{94}Mo	1.000	1.000	1.000	1.000	1.000	1.000	1.000	1.000	e
42	95	^{95}Mo	1.001	1.000	1.000	1.000	1.052	0.981	1.004	0.969	e
42	96	^{96}Mo	1.000	1.000	1.000	1.000	1.000	1.000	1.000	1.000	e
42	97	^{97}Mo	1.000	1.000	1.000	1.000	1.002	0.999	1.000	0.999	e
42	98	^{98}Mo	1.000	1.000	1.000	1.000	1.000	1.000	1.000	1.000	e
42	99	^{99}Mo	1.117	0.876	1.029	1.022	2.127	0.421	1.154	1.115	t
42	100	^{100}Mo	1.000	1.000	1.000	1.000	1.006	0.993	1.002	1.001	e
43	96	^{96}Tc	1.772	0.611	1.099	0.924	3.090	0.392	1.163	0.825	n,*
43	97	^{97}Tc	1.009	0.994	1.002	0.998	1.125	0.922	1.018	0.965	n
43	98	^{98}Tc	1.544	0.668	1.083	0.970	2.545	0.421	1.154	0.934	n,*
43	99	^{99}Tc	1.011	0.993	1.002	0.996	1.237	0.876	1.030	0.924	e
44	96	^{96}Ru	1.000	1.000	1.000	1.000	1.000	1.000	1.000	1.000	30
44	97	^{97}Ru	1.001	1.000	1.000	0.999	1.071	0.970	1.007	0.964	n
44	98	^{98}Ru	1.000	1.000	1.000	1.000	1.001	0.998	1.000	1.000	t
44	99	^{99}Ru	1.034	0.984	1.004	0.983	1.252	0.885	1.027	0.902	t
44	100	^{100}Ru	1.000	1.000	1.000	1.000	1.006	0.992	1.002	1.002	e
44	101	^{101}Ru	1.010	0.996	1.001	0.994	1.201	0.911	1.021	0.914	e
44	102	^{102}Ru	1.000	1.000	1.000	1.000	1.013	0.984	1.004	1.003	e
44	103	^{103}Ru	2.387	0.363	1.172	1.153	3.187	0.275	1.201	1.139	t,*
44	104	^{104}Ru	1.000	1.000	1.000	1.000	1.057	0.933	1.016	1.014	e
44	105	^{105}Ru	1.807	0.546	1.117	1.014	3.160	0.310	1.189	1.020	n,*

TABLE 1—Continued

Z	A	Nucl.	G_0^{30}	X^{30}	u_X^{30}	f_{SEF}^{30}	G_0^{80}	X^{80}	u_X^{80}	f_{SEF}^{80}	Comment ^a
44	106	¹⁰⁶ Ru	1.001	0.999	1.000	1.000	1.172	0.814	1.045	1.047	n
45	103	¹⁰³ Rh	2.287	0.385	1.165	1.136	5.088	0.180	1.233	1.091	e,*
45	104	¹⁰⁴ Rh	1.437	0.697	1.075	0.998	4.538	0.224	1.218	0.983	n,*
45	105	¹⁰⁵ Rh	1.012	0.991	1.002	0.997	1.254	0.833	1.040	0.957	n
46	102	¹⁰² Pd	1.000	1.000	1.000	1.000	1.005	0.995	1.001	1.001	30
46	103	¹⁰³ Pd	1.013	0.993	1.002	0.994	1.255	0.869	1.031	0.916	n
46	104	¹⁰⁴ Pd	1.000	1.000	1.000	1.000	1.005	0.993	1.002	1.003	e
46	105	¹⁰⁵ Pd	1.000	1.000	1.000	1.000	1.083	0.955	1.011	0.967	e
46	106	¹⁰⁶ Pd	1.000	1.000	1.000	1.000	1.008	0.988	1.003	1.004	e
46	107	¹⁰⁷ Pd	1.009	0.994	1.001	0.997	1.300	0.813	1.045	0.946	e
46	108	¹⁰⁸ Pd	1.000	1.000	1.000	1.000	1.022	0.971	1.007	1.008	e
46	109	¹⁰⁹ Pd	1.012	0.991	1.002	0.997	1.512	0.757	1.059	0.874	n
46	110	¹¹⁰ Pd	1.000	1.000	1.000	1.000	1.047	0.940	1.014	1.016	e
47	107	¹⁰⁷ Ag	1.256	0.753	1.060	1.057	3.340	0.262	1.205	1.142	e,*
47	108	¹⁰⁸ Ag	1.258	0.784	1.052	1.014	3.909	0.245	1.211	1.044	n,*
47	109	¹⁰⁹ Ag	1.273	0.944	1.013	0.832	3.342	0.727	1.067	0.411	e
47	110	¹¹⁰ Ag	2.743	0.332	1.182	1.099	4.711	0.188	1.231	1.131	t,*
47	111	¹¹¹ Ag	1.610	0.542	1.118	1.145	3.989	0.214	1.222	1.173	n,*
48	106	¹⁰⁶ Cd	1.000	1.000	1.000	1.000	1.002	0.997	1.001	1.001	e
48	107	¹⁰⁷ Cd	1.002	0.999	1.000	1.000	1.132	0.906	1.022	0.976	n
48	108	¹⁰⁸ Cd	1.000	1.000	1.000	1.000	1.002	0.997	1.001	1.001	e
48	109	¹⁰⁹ Cd	1.047	0.968	1.007	0.986	1.287	0.824	1.042	0.943	n
48	110	¹¹⁰ Cd	1.000	1.000	1.000	1.000	1.001	0.998	1.000	1.001	e
48	111	¹¹¹ Cd	1.001	0.999	1.000	1.000	1.236	0.794	1.050	1.019	e
48	112	¹¹² Cd	1.000	1.000	1.000	1.000	1.002	0.996	1.001	1.001	e
48	113	¹¹³ Cd	1.001	0.999	1.000	1.000	1.358	0.695	1.076	1.060	e
48	114	¹¹⁴ Cd	1.000	1.000	1.000	1.000	1.005	0.993	1.002	1.003	e
48	115	¹¹⁵ Cd	1.015	0.977	1.005	1.008	1.870	0.476	1.137	1.123	t
48	116	¹¹⁶ Cd	1.000	1.000	1.000	1.000	1.008	0.988	1.003	1.004	e
49	113	¹¹³ In	1.000	1.000	1.000	1.000	1.002	0.999	1.000	1.000	t
49	114	¹¹⁴ In	1.008	0.990	1.002	1.001	1.611	0.589	1.105	1.054	t
49	115	¹¹⁵ In	1.000	1.000	1.000	1.000	1.003	0.997	1.001	1.000	e
50	112	¹¹² Sn	1.000	1.000	1.000	1.000	1.000	1.000	1.000	1.000	e
50	114	¹¹⁴ Sn	1.000	1.000	1.000	1.000	1.000	1.000	1.000	1.000	e
50	115	¹¹⁵ Sn	1.000	1.000	1.000	1.000	1.007	0.991	1.002	1.002	e
50	116	¹¹⁶ Sn	1.000	1.000	1.000	1.000	1.000	1.000	1.000	1.000	e
50	117	¹¹⁷ Sn	1.010	0.991	1.002	0.999	1.394	0.686	1.078	1.046	e
50	118	¹¹⁸ Sn	1.000	1.000	1.000	1.000	1.000	1.000	1.000	1.000	e
50	119	¹¹⁹ Sn	2.205	0.390	1.164	1.162	4.444	0.151	1.244	1.493	e,*
50	120	¹²⁰ Sn	1.000	1.000	1.000	1.000	1.000	1.000	1.000	1.000	e
50	121	¹²¹ Sn	3.498	0.266	1.204	1.074	4.010	0.242	1.212	1.032	t,*

TABLE 1—Continued

<i>Z</i>	<i>A</i>	Nucl.	G_0^{30}	X^{30}	u_X^{30}	f_{SEF}^{30}	G_0^{80}	X^{80}	u_X^{80}	f_{SEF}^{80}	Comment ^a
50	122	^{122}Sn	1.000	1.000	1.000	1.000	1.000	1.000	1.000	1.000	e
50	123	^{123}Sn	1.148	0.875	1.030	0.996	1.271	0.795	1.050	0.990	n
50	124	^{124}Sn	1.000	1.000	1.000	1.000	1.000	1.000	1.000	1.000	e
50	125	^{125}Sn	1.133	0.881	1.028	1.001	1.248	0.803	1.048	0.998	t
50	126	^{126}Sn	1.000	1.000	1.000	1.000	1.000	1.000	1.000	1.000	t
51	121	^{121}Sb	1.387	0.724	1.068	0.996	1.840	0.528	1.122	1.029	30,*
51	122	^{122}Sb	1.342	0.762	1.058	0.978	3.978	0.268	1.203	0.938	t,*
51	123	^{123}Sb	1.004	0.998	1.001	0.999	1.102	0.938	1.015	0.968	30
51	125	^{125}Sb	1.000	1.000	1.000	1.000	1.012	0.994	1.002	0.995	t
51	126	^{126}Sb	1.486	0.638	1.091	1.054	2.095	0.494	1.132	0.966	n,*
51	127	^{127}Sb	1.000	1.000	1.000	1.000	1.002	0.999	1.000	0.999	n
52	120	^{120}Te	1.000	1.000	1.000	1.000	1.004	0.993	1.002	1.003	30
52	122	^{122}Te	1.000	1.000	1.000	1.000	1.004	0.994	1.002	1.002	e
52	123	^{123}Te	1.012	0.986	1.003	1.002	1.576	0.557	1.114	1.140	e
52	124	^{124}Te	1.000	1.000	1.000	1.000	1.003	0.996	1.001	1.002	e
52	125	^{125}Te	1.661	0.546	1.117	1.102	3.410	0.204	1.225	1.437	e,*
52	126	^{126}Te	1.000	1.000	1.000	1.000	1.001	0.998	1.000	1.001	e
52	127	^{127}Te	1.223	0.797	1.049	1.025	2.271	0.403	1.160	1.093	n,*
52	128	^{128}Te	1.000	1.000	1.000	1.000	1.000	0.999	1.000	1.000	e
52	130	^{130}Te	1.000	1.000	1.000	1.000	1.000	1.000	1.000	1.000	e
53	127	^{127}I	1.196	0.847	1.037	0.987	1.712	0.584	1.106	1.000	e
53	129	^{129}I	1.297	0.823	1.043	0.937	1.548	0.717	1.070	0.902	e,*
53	130	^{130}I	1.960	0.647	1.089	0.789	4.752	0.328	1.184	0.641	n,*
53	131	^{131}I	1.005	0.998	1.001	0.997	1.117	0.945	1.013	0.948	n
54	124	^{124}Xe	1.000	1.000	1.000	1.000	1.060	0.915	1.020	1.031	30
54	126	^{126}Xe	1.000	1.000	1.000	1.000	1.039	0.940	1.014	1.024	30
54	128	^{128}Xe	1.000	1.000	1.000	1.000	1.020	0.970	1.007	1.011	30
54	129	^{129}Xe	1.537	0.608	1.100	1.071	2.820	0.271	1.202	1.309	30,*
54	130	^{130}Xe	1.000	1.000	1.000	1.000	1.006	0.990	1.002	1.003	30
54	131	^{131}Xe	1.047	0.965	1.008	0.989	1.629	0.564	1.112	1.089	t
54	132	^{132}Xe	1.000	1.000	1.000	1.000	1.001	0.998	1.000	1.001	e
54	133	^{133}Xe	1.001	0.998	1.000	1.001	1.185	0.801	1.048	1.053	t
54	134	^{134}Xe	1.000	1.000	1.000	1.000	1.000	1.000	1.000	1.000	30
54	136	^{136}Xe	1.000	1.000	1.000	1.000	1.000	1.000	1.000	1.000	e
55	133	^{133}Cs	1.054	0.966	1.008	0.983	1.379	0.818	1.044	0.886	e
55	134	^{134}Cs	1.973	0.510	1.127	0.993	3.305	0.305	1.191	0.991	t,*
55	135	^{135}Cs	1.000	1.000	1.000	1.000	1.049	0.972	1.007	0.981	30
55	136	^{136}Cs	1.043	0.832	1.040	1.152	1.359	0.610	1.099	1.206	n,*
55	137	^{137}Cs	1.000	1.000	1.000	1.000	1.003	0.999	1.000	0.999	n
56	130	^{130}Ba	1.000	1.000	1.000	1.000	1.065	0.907	1.022	1.035	30
56	132	^{132}Ba	1.000	1.000	1.000	1.000	1.015	0.980	1.005	1.005	30

TABLE 1—Continued

Z	A	Nucl.	G_0^{30}	X^{30}	u_X^{30}	f_{SEF}^{30}	G_0^{80}	X^{80}	u_X^{80}	f_{SEF}^{80}	Comment ^a
56	134	^{134}Ba	1.000	1.000	1.000	1.000	1.003	0.996	1.001	1.001	e
56	135	^{135}Ba	1.001	0.999	1.000	1.000	1.141	0.818	1.044	1.071	e
56	136	^{136}Ba	1.000	1.000	1.000	1.000	1.000	1.000	1.000	1.000	e
56	137	^{137}Ba	1.000	1.000	1.000	1.000	1.016	0.994	1.001	0.991	e
56	138	^{138}Ba	1.000	1.000	1.000	1.000	1.000	1.000	1.000	1.000	e
57	138	^{138}La	1.070	0.949	1.012	0.984	1.550	0.768	1.056	0.839	t
57	139	^{139}La	1.003	0.999	1.000	0.998	1.094	0.955	1.010	0.957	e
57	140	^{140}La	2.439	0.485	1.135	0.846	5.104	0.238	1.213	0.822	n,*
58	132	^{132}Ce	1.000	1.000	1.000	1.000	1.086	0.882	1.028	1.044	t
58	133	^{133}Ce	2.482	0.294	1.195	1.370	5.223	0.133	1.250	1.440	t,*
58	134	^{134}Ce	1.000	1.000	1.000	1.000	1.030	0.954	1.011	1.018	t
58	135	^{135}Ce	1.127	0.874	1.030	1.015	1.827	0.489	1.134	1.119	t
58	136	^{136}Ce	1.000	1.000	1.000	1.000	1.005	0.992	1.002	1.003	30
58	137	^{137}Ce	1.003	0.997	1.001	1.000	1.203	0.747	1.062	1.113	t
58	138	^{138}Ce	1.000	1.000	1.000	1.000	1.000	1.000	1.000	1.000	30
58	139	^{139}Ce	1.000	1.000	1.000	1.000	1.021	0.991	1.002	0.988	t
58	140	^{140}Ce	1.000	1.000	1.000	1.000	1.000	1.000	1.000	1.000	e
58	141	^{141}Ce	1.000	1.000	1.000	1.000	1.000	1.000	1.000	1.000	t
58	142	^{142}Ce	1.000	1.000	1.000	1.000	1.002	0.997	1.001	1.001	30
58	143	^{143}Ce	2.431	0.358	1.174	1.149	3.464	0.207	1.224	1.395	n,*
59	141	^{141}Pr	1.010	0.991	1.002	0.998	1.217	0.829	1.041	0.992	e
59	142	^{142}Pr	4.406	0.203	1.226	1.120	8.179	0.122	1.254	1.002	t,*
59	143	^{143}Pr	1.111	0.933	1.016	0.965	1.375	0.800	1.048	0.910	t
60	142	^{142}Nd	1.000	1.000	1.000	1.000	1.000	1.000	1.000	1.000	e
60	143	^{143}Nd	1.000	1.000	1.000	1.000	1.000	1.000	1.000	1.000	e
60	144	^{144}Nd	1.000	1.000	1.000	1.000	1.001	0.998	1.000	1.001	e
60	145	^{145}Nd	1.120	0.943	1.013	0.947	1.520	0.793	1.050	0.830	e
60	146	^{146}Nd	1.000	1.000	1.000	1.000	1.017	0.977	1.005	1.006	e
60	147	^{147}Nd	1.270	0.807	1.047	0.976	2.112	0.487	1.134	0.971	t,*
60	148	^{148}Nd	1.000	1.000	1.000	1.000	1.116	0.884	1.027	1.013	e
60	150	^{150}Nd	1.065	0.926	1.017	1.014	2.061	0.423	1.154	1.147	e
61	147	^{147}Pm	1.057	0.963	1.009	0.983	1.672	0.660	1.085	0.907	30
61	148	^{148}Pm	1.165	0.854	1.035	1.005	4.622	0.200	1.226	1.081	t
61	149	^{149}Pm	1.019	0.988	1.003	0.993	1.464	0.786	1.052	0.869	t
62	144	^{144}Sm	1.000	1.000	1.000	1.000	1.000	1.000	1.000	1.000	e
62	147	^{147}Sm	1.014	0.992	1.002	0.995	1.208	0.890	1.026	0.931	e
62	148	^{148}Sm	1.000	1.000	1.000	1.000	1.005	0.992	1.002	1.003	e
62	149	^{149}Sm	1.354	0.803	1.048	0.919	1.634	0.682	1.079	0.897	e,*
62	150	^{150}Sm	1.000	1.000	1.000	1.000	1.078	0.913	1.021	1.017	e
62	151	^{151}Sm	1.945	0.585	1.106	0.879	4.595	0.244	1.211	0.892	e,*
62	152	^{152}Sm	1.086	0.890	1.026	1.035	2.185	0.363	1.172	1.259	e

TABLE 1—Continued

Z	A	Nucl.	G_0^{30}	X^{30}	u_X^{30}	f_{SEF}^{30}	G_0^{80}	X^{80}	u_X^{80}	f_{SEF}^{80}	Comment ^a
62	153	^{153}Sm	3.321	0.243	1.212	1.241	8.509	0.086	1.267	1.364	t,*
62	154	^{154}Sm	1.326	0.670	1.083	1.126	3.129	0.219	1.220	1.459	e,*
63	151	^{151}Eu	1.656	0.582	1.107	1.037	2.506	0.379	1.167	1.052	e,*
63	152	^{152}Eu	1.557	0.706	1.073	0.910	8.333	0.165	1.239	0.730	t,*
63	153	^{153}Eu	1.158	0.884	1.027	0.976	2.650	0.441	1.148	0.856	e
63	154	^{154}Eu	1.415	0.752	1.061	0.940	5.848	0.223	1.219	0.768	30,*
63	155	^{155}Eu	1.138	0.893	1.025	0.985	2.332	0.473	1.138	0.906	30
63	156	^{156}Eu	4.159	0.170	1.237	1.413	19.94	0.033	1.287	1.523	n,*
64	152	^{152}Gd	1.000	1.000	1.000	1.000	1.069	0.908	1.022	1.030	e
64	153	^{153}Gd	1.681	0.580	1.107	1.026	6.064	0.162	1.240	1.020	t,*
64	154	^{154}Gd	1.083	0.880	1.029	1.050	2.163	0.352	1.176	1.312	e
64	155	^{155}Gd	1.499	0.662	1.085	1.008	5.528	0.180	1.233	1.006	e,*
64	156	^{156}Gd	1.258	0.703	1.074	1.131	2.898	0.239	1.213	1.442	e,*
64	157	^{157}Gd	1.497	0.685	1.078	0.975	3.930	0.256	1.207	0.993	e,*
64	158	^{158}Gd	1.355	0.652	1.087	1.132	3.209	0.211	1.223	1.478	e,*
64	159	^{159}Gd	1.527	0.675	1.081	0.971	4.296	0.250	1.209	0.932	n,*
64	160	^{160}Gd	1.409	0.629	1.094	1.128	3.375	0.196	1.228	1.509	n,*
65	157	^{157}Tb	1.214	0.817	1.044	1.008	2.282	0.413	1.157	1.060	n,*
65	158	^{158}Tb	1.339	0.743	1.063	1.005	3.227	0.321	1.186	0.965	n,*
65	159	^{159}Tb	1.238	0.785	1.052	1.029	2.327	0.398	1.161	1.079	e,*
65	160	^{160}Tb	1.382	0.747	1.062	0.969	3.993	0.302	1.192	0.829	t,*
65	161	^{161}Tb	1.254	0.793	1.050	1.006	2.333	0.402	1.160	1.067	n,*
66	156	^{156}Dy	1.051	0.922	1.018	1.033	1.952	0.401	1.160	1.278	30
66	158	^{158}Dy	1.185	0.820	1.043	1.030	2.628	0.290	1.196	1.311	t,*
66	159	^{159}Dy	1.256	0.790	1.051	1.008	2.908	0.338	1.180	1.017	n,*
66	160	^{160}Dy	1.278	0.696	1.075	1.125	2.958	0.234	1.215	1.442	e,*
66	161	^{161}Dy	1.913	0.530	1.122	0.987	4.433	0.232	1.215	0.972	e,*
66	162	^{162}Dy	1.341	0.636	1.092	1.173	3.162	0.212	1.222	1.493	e,*
66	163	^{163}Dy	1.122	0.896	1.025	0.994	1.965	0.534	1.120	0.953	e
66	164	^{164}Dy	1.436	0.596	1.103	1.168	3.459	0.189	1.230	1.528	e,*
67	163	^{163}Ho	1.046	0.959	1.009	0.997	1.521	0.676	1.081	0.973	30
67	165	^{165}Ho	1.055	0.950	1.012	0.999	1.539	0.670	1.082	0.970	e
67	166	^{166}Ho	14.53	0.042	1.284	1.648	26.69	0.023	1.291	1.602	n,*
68	162	^{162}Er	1.167	0.784	1.053	1.094	2.547	0.291	1.195	1.347	30,*
68	164	^{164}Er	1.238	0.745	1.062	1.084	2.815	0.268	1.203	1.328	30,*
68	166	^{166}Er	1.342	0.636	1.092	1.172	3.168	0.214	1.221	1.472	e,*
68	167	^{167}Er	1.093	0.930	1.016	0.983	1.770	0.598	1.102	0.944	e
68	168	^{168}Er	1.351	0.653	1.087	1.133	3.190	0.211	1.223	1.485	e,*
68	169	^{169}Er	1.638	0.611	1.099	0.999	5.473	0.172	1.236	1.064	t,*
68	170	^{170}Er	1.366	0.651	1.088	1.125	3.236	0.205	1.225	1.506	e,*
69	169	^{169}Tm	2.609	0.304	1.191	1.260	4.582	0.159	1.241	1.375	e,*

TABLE 1—Continued

Z	A	Nucl.	G_0^{30}	X^{30}	u_X^{30}	f_{SEF}^{30}	G_0^{80}	X^{80}	u_X^{80}	f_{SEF}^{80}	Comment ^a
69	170	^{170}Tm	1.529	0.618	1.097	1.058	4.041	0.237	1.214	1.046	t,*
69	171	^{171}Tm	2.808	0.263	1.205	1.356	4.573	0.144	1.246	1.521	t,*
69	172	^{172}Tm	1.189	0.841	1.038	1.000	2.015	0.486	1.135	1.021	n
70	168	^{168}Yb	1.269	0.713	1.071	1.105	2.930	0.251	1.209	1.361	30,*
70	170	^{170}Yb	1.302	0.667	1.083	1.151	3.034	0.230	1.216	1.433	e,*
70	171	^{171}Yb	1.700	0.551	1.116	1.067	6.731	0.129	1.252	1.151	e,*
70	172	^{172}Yb	1.364	0.624	1.095	1.174	3.233	0.207	1.224	1.497	e,*
70	173	^{173}Yb	1.101	0.916	1.020	0.991	1.768	0.578	1.108	0.979	e
70	174	^{174}Yb	1.392	0.633	1.092	1.134	3.320	0.198	1.227	1.519	e,*
70	175	^{175}Yb	1.039	0.968	1.008	0.994	1.500	0.715	1.071	0.933	t
70	176	^{176}Yb	1.325	0.673	1.082	1.121	3.104	0.214	1.222	1.508	e,*
71	175	^{175}Lu	1.028	0.975	1.006	0.998	1.427	0.728	1.067	0.963	e
71	176	$^{176}\text{Lu}^b$	1.006	0.995	1.001	0.999	1.286	0.830	1.041	0.937	e
71	177	^{177}Lu	1.030	0.975	1.006	0.996	1.576	0.695	1.076	0.912	n
72	174	^{174}Hf	1.241	0.730	1.067	1.104	2.828	0.260	1.206	1.359	30,*
72	176	^{176}Hf	1.264	0.719	1.069	1.101	2.905	0.244	1.211	1.408	e,*
72	177	^{177}Hf	1.029	0.973	1.006	0.999	1.418	0.724	1.068	0.973	e
72	178	^{178}Hf	1.224	0.740	1.064	1.104	2.759	0.257	1.207	1.413	e,*
72	179	^{179}Hf	1.021	0.986	1.003	0.994	1.395	0.763	1.058	0.939	e
72	180	^{180}Hf	1.223	0.750	1.061	1.090	2.752	0.258	1.207	1.410	e,*
72	181	^{181}Hf	1.552	0.605	1.100	1.065	3.611	0.215	1.221	1.285	t,*
72	182	^{182}Hf	1.192	0.780	1.053	1.075	2.636	0.268	1.203	1.418	30,*
73	179	^{179}Ta	1.468	0.677	1.081	1.007	2.365	0.434	1.150	0.974	t,*
73	180	$^{180}\text{Ta}^b$	2.037	0.437	1.149	1.122	7.168	0.109	1.259	1.281	e,*
73	181	^{181}Ta	2.038	0.478	1.137	1.028	2.660	0.378	1.168	0.995	e,*
73	182	^{182}Ta	2.014	0.492	1.133	1.008	3.987	0.285	1.197	0.879	t,*
73	183	^{183}Ta	1.124	0.909	1.021	0.979	1.952	0.547	1.117	0.938	n
74	180	^{180}W	1.159	0.805	1.047	1.072	2.506	0.301	1.192	1.324	30,*
74	182	^{182}W	1.178	0.793	1.050	1.070	2.580	0.284	1.198	1.366	e,*
74	183	^{183}W	1.541	0.599	1.102	1.083	3.827	0.206	1.224	1.265	e,*
74	184	^{184}W	1.123	0.841	1.038	1.059	2.342	0.320	1.186	1.335	30
74	185	^{185}W	1.454	0.751	1.061	0.916	3.217	0.315	1.188	0.989	30,*
74	186	^{186}W	1.084	0.905	1.022	1.019	2.145	0.380	1.167	1.227	30
74	187	^{187}W	1.121	0.897	1.024	0.994	2.004	0.513	1.127	0.973	n
75	185	^{185}Re	1.020	0.981	1.004	0.999	1.351	0.744	1.063	0.996	30
75	186	^{186}Re	1.396	0.689	1.077	1.039	5.199	0.168	1.238	1.145	t,*
75	187	^{187}Re	1.017	0.987	1.003	0.996	1.432	0.723	1.068	0.966	30
75	188	^{188}Re	1.237	0.795	1.050	1.017	3.349	0.263	1.205	1.134	n,*
75	189	^{189}Re	1.036	0.964	1.008	1.001	1.640	0.620	1.096	0.984	n
76	184	^{184}Os	1.092	0.884	1.027	1.036	2.194	0.362	1.173	1.260	30
76	186	^{186}Os	1.052	0.917	1.020	1.037	1.940	0.410	1.158	1.257	e

TABLE 1—Continued

Z	A	Nucl.	G_0^{30}	X^{30}	u_X^{30}	f_{SEF}^{30}	G_0^{80}	X^{80}	u_X^{80}	f_{SEF}^{80}	Comment ^a
76	187	^{187}Os	3.016	0.278	1.200	1.193	7.184	0.104	1.260	1.333	e,*
76	188	^{188}Os	1.028	0.957	1.010	1.016	1.746	0.474	1.138	1.209	e
76	189	^{189}Os	2.356	0.384	1.166	1.105	5.402	0.153	1.243	1.209	e,*
76	190	^{190}Os	1.010	0.985	1.004	1.006	1.500	0.580	1.107	1.150	30
76	191	^{191}Os	1.060	0.967	1.008	0.976	1.639	0.750	1.061	0.813	t
76	192	^{192}Os	1.005	0.993	1.002	1.002	1.401	0.658	1.086	1.085	30
76	193	^{193}Os	1.290	0.844	1.037	0.918	2.281	0.486	1.134	0.901	n
76	194	^{194}Os	1.003	0.995	1.001	1.001	1.333	0.691	1.077	1.085	n
77	191	^{191}Ir	1.065	0.949	1.012	0.990	2.015	0.473	1.139	1.050	e
77	192	^{192}Ir	3.065	0.331	1.183	0.986	6.000	0.183	1.232	0.910	t,*
77	193	^{193}Ir	1.268	0.747	1.062	1.056	2.794	0.299	1.193	1.197	e,*
77	194	^{194}Ir	1.349	0.789	1.051	0.940	4.830	0.222	1.219	0.931	n,*
78	190	^{190}Pt	1.000	1.000	1.000	1.000	1.128	0.845	1.037	1.050	30
78	192	^{192}Pt	1.000	1.000	1.000	1.000	1.099	0.869	1.031	1.048	30
78	193	^{193}Pt	4.881	0.156	1.242	1.312	8.241	0.080	1.270	1.517	t,*
78	194	^{194}Pt	1.000	1.000	1.000	1.000	1.085	0.890	1.026	1.035	t
78	195	^{195}Pt	1.121	0.888	1.026	1.004	3.119	0.288	1.197	1.112	t
78	196	^{196}Pt	1.000	1.000	1.000	1.000	1.060	0.925	1.018	1.021	30
78	197	^{197}Pt	1.783	0.536	1.120	1.046	4.332	0.193	1.229	1.197	n,*
78	198	^{198}Pt	1.000	1.000	1.000	1.000	1.031	0.964	1.008	1.006	30
79	195	^{195}Au	1.065	0.962	1.009	0.976	1.403	0.750	1.061	0.950	n
79	196	^{196}Au	1.677	0.631	1.093	0.945	3.512	0.298	1.193	0.956	n,*
79	197	^{197}Au	1.038	0.983	1.004	0.980	1.294	0.841	1.038	0.919	e
79	198	^{198}Au	1.108	0.944	1.013	0.956	1.858	0.665	1.084	0.809	t
79	199	^{199}Au	1.038	0.988	1.003	0.975	1.246	0.897	1.024	0.895	n
80	196	^{196}Hg	1.000	1.000	1.000	1.000	1.024	0.963	1.009	1.014	30
80	198	^{198}Hg	1.000	1.000	1.000	1.000	1.029	0.961	1.009	1.011	e
80	199	^{199}Hg	1.017	0.978	1.005	1.005	1.611	0.590	1.104	1.052	e
80	200	^{200}Hg	1.000	1.000	1.000	1.000	1.050	0.941	1.014	1.012	e
80	201	^{201}Hg	2.442	0.449	1.146	0.911	3.332	0.282	1.199	1.064	e,*
80	202	^{202}Hg	1.000	1.000	1.000	1.000	1.021	0.979	1.005	1.000	30
80	203	^{203}Hg	1.383	0.832	1.040	0.869	1.731	0.733	1.066	0.789	t,*
80	204	^{204}Hg	1.000	1.000	1.000	1.000	1.021	0.982	1.004	0.997	30
81	203	^{203}Tl	1.000	1.000	1.000	1.000	1.062	0.949	1.012	0.992	e
81	204	^{204}Tl	1.007	0.998	1.001	0.995	1.170	0.932	1.016	0.917	t
81	205	^{205}Tl	1.002	0.998	1.000	0.999	1.158	0.899	1.024	0.960	e
82	204	^{204}Pb	1.000	1.000	1.000	1.000	1.000	1.000	1.000	1.000	e
82	205	^{205}Pb	1.309	0.824	1.042	0.927	1.350	0.836	1.039	0.886	t,*
82	206	^{206}Pb	1.000	1.000	1.000	1.000	1.000	1.000	1.000	1.000	e
82	207	^{207}Pb	1.000	1.000	1.000	1.000	1.002	0.998	1.001	1.000	e
82	208	^{208}Pb	1.000	1.000	1.000	1.000	1.000	1.000	1.000	1.000	e

TABLE 1—*Continued*

<i>Z</i>	<i>A</i>	Nucl.	G_0^{30}	X^{30}	u_X^{30}	f_{SEF}^{30}	G_0^{80}	X^{80}	u_X^{80}	f_{SEF}^{80}	Comment ^a
83	209	^{209}Bi	1.000	1.000	1.000	1.000	1.000	1.000	1.000	1.000	e
83	210	^{210}Bi	1.072	0.981	1.004	0.951	1.514	0.625	1.095	1.056	t

^aThe marks appearing in the comments refer to KADoNiS v0.3 (Dillmann et al. 2009): n (not present), t (only theoretical estimate), 30 (only 30 keV MACS), e (measured in the relevant energy range), * ($X_{\text{lower}}^{30} < 0.8$, appearing in figure 4).

^b X and f_{SEF} given for the g.s., not the isomeric state, and assuming thermal equilibration of g.s. and excited states.